JACS Au
AN OPEN ACCESS JOURNAL OF THE AMERICAN CHEMICAL SOCIETY

pubs.acs.org/jacsau
Article

Sulfonated Microporous Polyxanthene Binder for High-Temperature Hydrogen Fuel Cells

Published as part of JACS Au special issue "Polymers for the Clean Energy Transition".

Shuo Yang,[⊥] Hui Li,[⊥] Wenhao Zou, Rene Ling, Xinchi Ma, Siyu Chen, Zhengjin Yang,* and Tongwen Xu*

Cite This: *JACS Au* 2024, 4, 3277−3283
Read Online

ACCESS | Metrics & More | Article Recommendations | Supporting Information

ABSTRACT: High-temperature proton exchange membrane fuel cells based on phosphoric acid-doped polybenzimidazole (PBI) materials face challenges of low power output and low Pt utilization due to the lack of suitable electrode binders. We have developed a sulfonated microporous polymer material (namely, SPX, i.e., sulfonated polyxanthene) with excellent chemical stability, to be used as the electrode binder. The rigid and contorted polymer structure of SPX reduces the adsorption of the ionomer on the Pt catalyst surface, prevents phosphoric acid loss, and promotes the rapid transport of reactant gases and water molecules within the catalyst layer. The cell performance is thereby significantly improved, with a Pt utilization reaching 42.51%, and a peak power density approaching 805 mW cm^{-2} at 180 °C, surpassing the performance of cells using PBI as a binder.

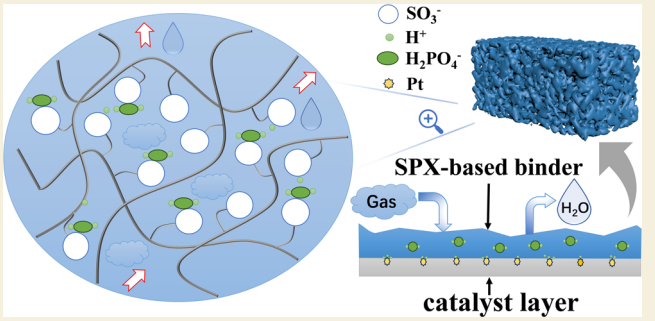

KEYWORDS: *high-temperature proton exchange membrane fuel cell, binder, sulfonated polyxanthene, catalyst layer, adsorption*

INTRODUCTION

High-temperature H_2/O_2 proton exchange membrane fuel cells (HT-PEMFCs) based on a phosphoric acid-doped polybenzimidazole (PA−PBI) membrane represent the most mature fuel cell technology in the operating temperature range of 140 to 180 °C.[1−3] However, the inefficiency of gas transport within the catalyst layer and low Pt utilization result in a relatively low power output and require a high Pt catalyst loading. At 160 °C, the electrodes used in this scheme typically contain 0.7 mg_{pt} cm^{-2} of Pt, which delivers a peak power density of around 350 mW cm^{-2} that does not meet the requirements of long-haul transportation.[3] This significantly increases the cost of this technology due to a low Pt-specific power density and low Pt utilization. To our knowledge, the Pt utilization of PA−PBI HT-PEMFCs is at merely about 15%, far below the approximately 75% utilization in low-temperature fuel cells.[4,5]

Identifying key factors that may help improve Pt utilization and improve the HT-PEMFC power output is critical. In a membrane electrode assembly (MEA), besides the proton exchange membrane, the ionomeric binder is another critical component.[6] In the MEA catalyst layer, the ionomeric binder coats the Pt catalyst surface, forming a thin layer with an average thickness of 6−13 nm.[7,8] The thin layer acts as a binder for the catalyst particles and participates in electrochemical reactions by regulating the mass transport at the electrode.

A common theme in the efforts to use PA−PBI as an ionomer in the catalyst layer has been to find an optimal balance that ensures proton conduction without obstructing material transport. For instance, Mamlou and Scott[9] optimized the performance of HT-PEMFC cells by varying the PBI content and the acid doping level within the electrode. The optimized cells present a peak power density of about 500 mW cm^{-2} at an operating temperature of 175 °C. However, the conventional practice of using the same polymer (for instance, polybenzimidazole) as both the proton exchange membrane and the electrode ionomeric binder in the membrane electrode assembly does not account for their drastically different requirements on gas permeability. The binder shall allow low-resistance permeation of reactant gases and product water, while the membrane should prevent the cross-membrane mixing of H_2 with O_2.[10] In addition, the adsorption of aromatic groups of ionomeric binders on the Pt catalyst surface will seriously compromise the cell performance.[11]

Received: June 29, 2024
Revised: August 7, 2024
Accepted: August 7, 2024
Published: August 15, 2024

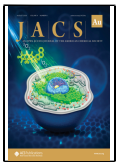

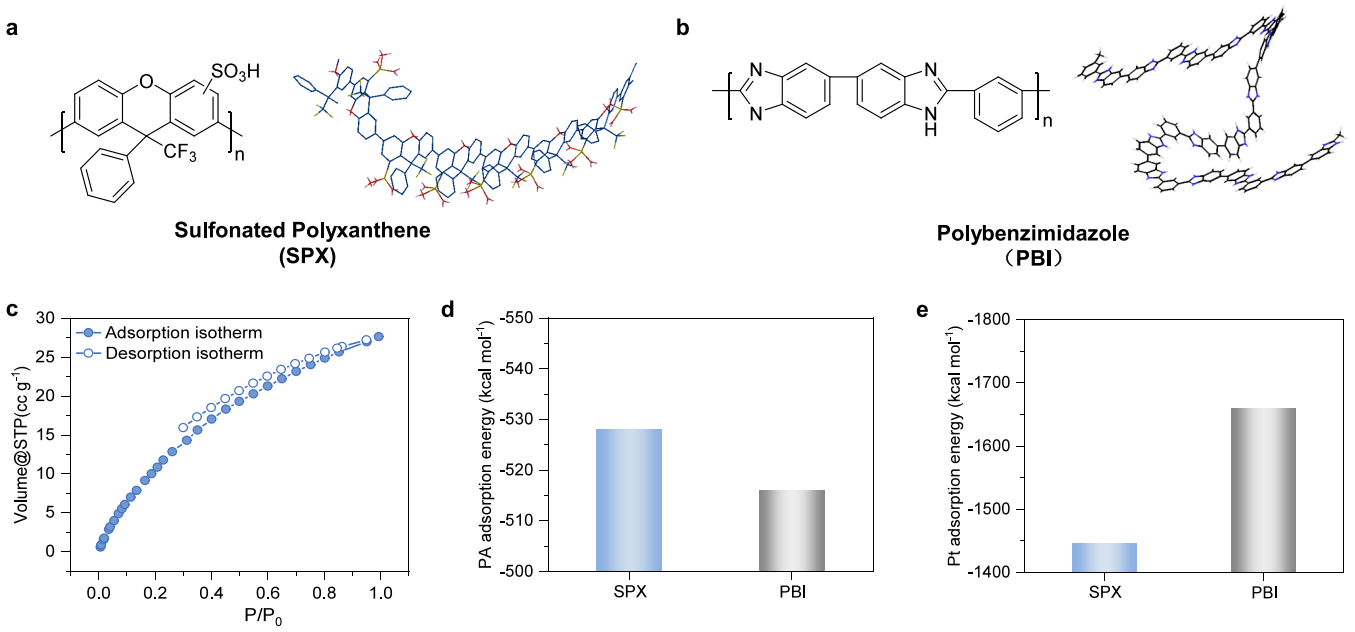

Figure 1. Properties of intrinsically microporous sulfonated ionomeric binders. Chemical structures and molecular configurations of (a) SPX and (b) PBI control. (c) CO_2 sorption adsorption−desorption isotherms of the SPX ionomer (at 273.15 K). Density functional theory (DFT) optimized interaction energy (d) of PA with SPX or PBI and adsorption energy (e) of SPX and PBI ionomers on the Pt catalyst surface (for calculation, the system consists of an ionomer, Pt catalyst, and PA).

An ideal ionomeric binder shall have high proton conductivity as well as high permeability to gaseous reactants and produced water.[12] The adsorption of the ionomeric binder on the Pt surface should be mitigated to achieve high Pt utilization. For PA-doped binders, the interaction between the ionomeric binder and PA should also be examined since PA as a proton carrier can promote proton conduction and is crucial in constructing a good three-phase interface.

Ionomeric binders derived from microporous polymer materials have recently raised broad research interest. Li et al.[13] reported an effective catalyst binder material based on intrinsic microporous polymers (PIMs) with strong hydrogen bond functionality for HT-PEMFCs. They found that effective catalyst binders based on PIMs[14] can form strong hydrogen-bonding interactions that improve phosphoric acid retention and improve mass transport at the electrode. The tetrazole-functionalized PIM binder enables a H_2/O_2 cell to achieve a high Pt mass-specific peak power density of 3.8 W mg_{Pt}^{-1} at 160 °C, with a Pt loading of 0.15 mg_{Pt} cm^{-2}. However, the Pt utilization of this work was still not high (at ∼25%). Wang et al.[15] customized the three-phase microenvironment of low-temperature H_2/O_2 fuel cells by adding ionic covalent organic framework (COF) nanosheets to Nafion to optimize the ionomer. The Pt mass activity and peak power density (at a cathode Pt loading of 0.07 mg $_{Pt}$/ cm^2) of the resultant cells are 1.6 times higher than those of an otherwise identical cell without COF nanosheets.

Here, we report a chemically stable sulfonated polyxanthene (SPX) as the ionomeric binder for HT-PEMFCs, which have abundant micropore channels. The sulfonic acid groups ensured rapid proton conduction within the channels. The simulation results show that the rigid and twisted molecular configuration reduces the adsorption of the ionomer on the catalyst surface and the presence of microporous channels enhances the retention of phosphoric acid. Benefiting from the microporous structure, SPX allows for rapid material mass transport in the catalyst layer. With the SPX ionomer, the H_2/O_2 fuel cell achieves a Pt utilization reaching 42.51% and improves the peak power density to 805 mW cm^{-2} at 180 °C. In addition, we also found that the fuel cell performance degraded at more than 180 °C or low Pt loading conditions and preliminarily explored the cause. Therefore, the strategy that we propose in the present work can achieve excellent power density and Pt utilization for H_2/O_2 HT-PEMFCs, which will be beneficial to the further application of H_2/O_2 HT-PEMFCs.

RESULTS AND DISCUSSION

Synthesis and Characterization of Microporous Polymers

We synthesized a polyxanthene polymer with 4,4′-dihydroxybiphenyl and 2,2,2-trifluoroacetophenone via a superacid-catalyzed polycondensation reaction (designated as PX, Figure S1a), according to a reported procedure.[16,17] PX was then sulfonated, resulting in a sulfonated ionomer designated as SPX (Figure 1a). The successful synthesis of PX and SPX was confirmed by the NMR spectra (Figure S1).

The rigid backbone and partial fluorinated structure of PX and SPX enable them to be readily soluble in dimethyl sulfoxide, forming a homogeneous solution[16] and benefiting the subsequent use as an ionomeric binder material in membrane electrode assembly (MEA). The rigid and contorted polymer backbone of SPX prevents effective polymer chain packing, as revealed by molecular simulations (Figure 1a). The SPX polymer chain displays a twisted molecular conformation and cannot be densely packed, whereas the control PBI chains are more flexible and can pack efficiently (Figure 1b).

N_2 adsorption−desorption isotherms at 77.3 K were used to analyze the microporous structure of the PX polymer (Figure S2), and the calculated BET surface area of PX was approximately 294.3 m^2 g^{-1}. By contrast, the presence of

https://doi.org/10.1021/jacsau.4c00565
JACS Au 2024, 4, 3277−3283

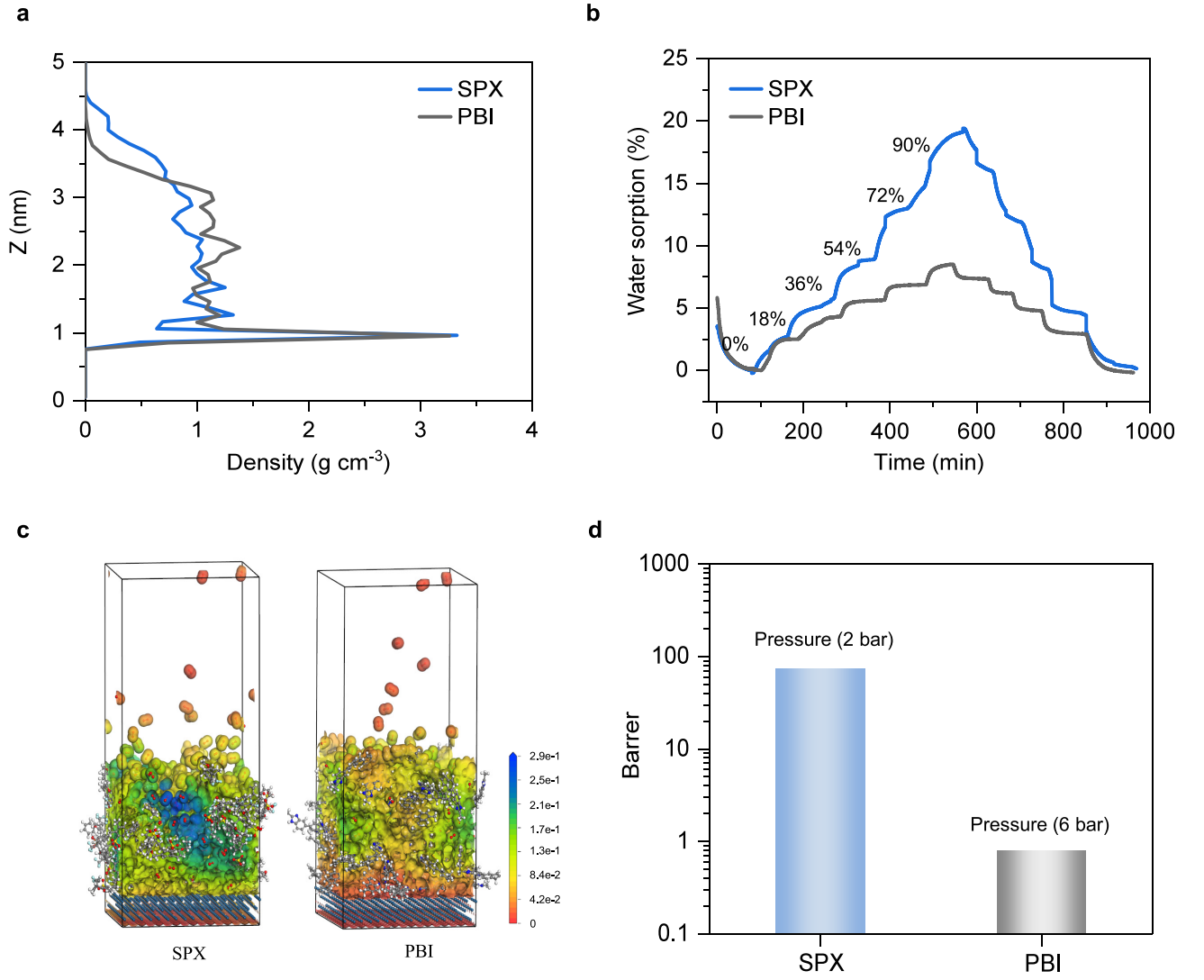

Figure 2. Improved electrode triple-phase interface by the SPX ionomer. (a) Density distribution profiles recorded for SPX and PBI near the Pt surface (0−5 nm) during molecular dynamics simulations. (b) Dynamic water vapor sorption (DVS) isotherms of SPX and PBI ionomers, measured at 25 °C and varied relative humidity (labels above the curves). (c) Three-dimensional equilibrated oxygen distribution at the ionomer−Pt vicinity as derived from molecular dynamic simulations. The ionomers include SPX and PBI. Regions with higher O_2 concentrations are colored blue. (d) Oxygen permeability across the SPX and PBI ionomers.

sulfonic acid groups within SPX resulted in hydrogen bonding between sulfonate groups, leading to stronger interchain and intrachain interactions and preventing the N_2 molecules from entering the free volume elements. Therefore, the free volume of SPX was probed by the CO_2 adsorption−desorption experiments. Based on the CO_2 adsorption−desorption isotherms (Figure 1c), density functional theory (DFT) calculations revealed that SPX has a micropore free volume of 0.091 $cm^3\ g^{-1}$ and a pore size distribution ranging from 0.45 to 0.9 nm (Figure S3), indicating the microporous structure of the sulfonated polymer.[18]

SPX can form strong interactions with PA,[13] but not with Pt, as revealed by DFT calculations. Our calculation results showed that the interaction energy between SPX and PA is −528 kcal mol^{-1}, higher than that for PBI (Figure 1d). This can be explained by the hydrogen bonds formed between PA and the sulfonic acid groups of SPX within its micropores, which strongly adsorb PA molecules. By contrast, only acid−base interactions are present between the benzimidazole units and PA. This implies the strong confinement effect of micropore free volume elements and may help prevent PA loss during battery operation. DFT calculations also suggested that the extremely rigid and twisted molecular conformation of SPX could mitigate the adsorption of ionomer on the Pt catalyst surface (Figure S4, Figure 1e).

Mass Transport within Gas Diffusion Electrodes

To compare SPX with the PBI control, we fabricated gas diffusion electrodes (GDEs) with both ionomeric binders and analyzed the pore volumes of GDEs. The SPX-based GDE had a pore volume of 1.48 mL g^{-1}, compared to a value of 1.30 mL g^{-1} for the PBI-based GDE (Figure S5). Scanning electron microscopy (SEM) images revealed that the surfaces of both the SPX-based GDE and PBI-based GDE were smooth and free of cracks (Figure S6). In addition, we find that the SPX-based GDE exhibited more uniform catalyst particle distribution without agglomerations, as compared to the PBI-based GDE following the same preparation procedure. To note, our simulated distribution of ionomers on the Pt catalyst surface (Figure S7) and the density distribution curves near the

https://doi.org/10.1021/jacsau.4c00565
JACS Au 2024, 4, 3277−3283

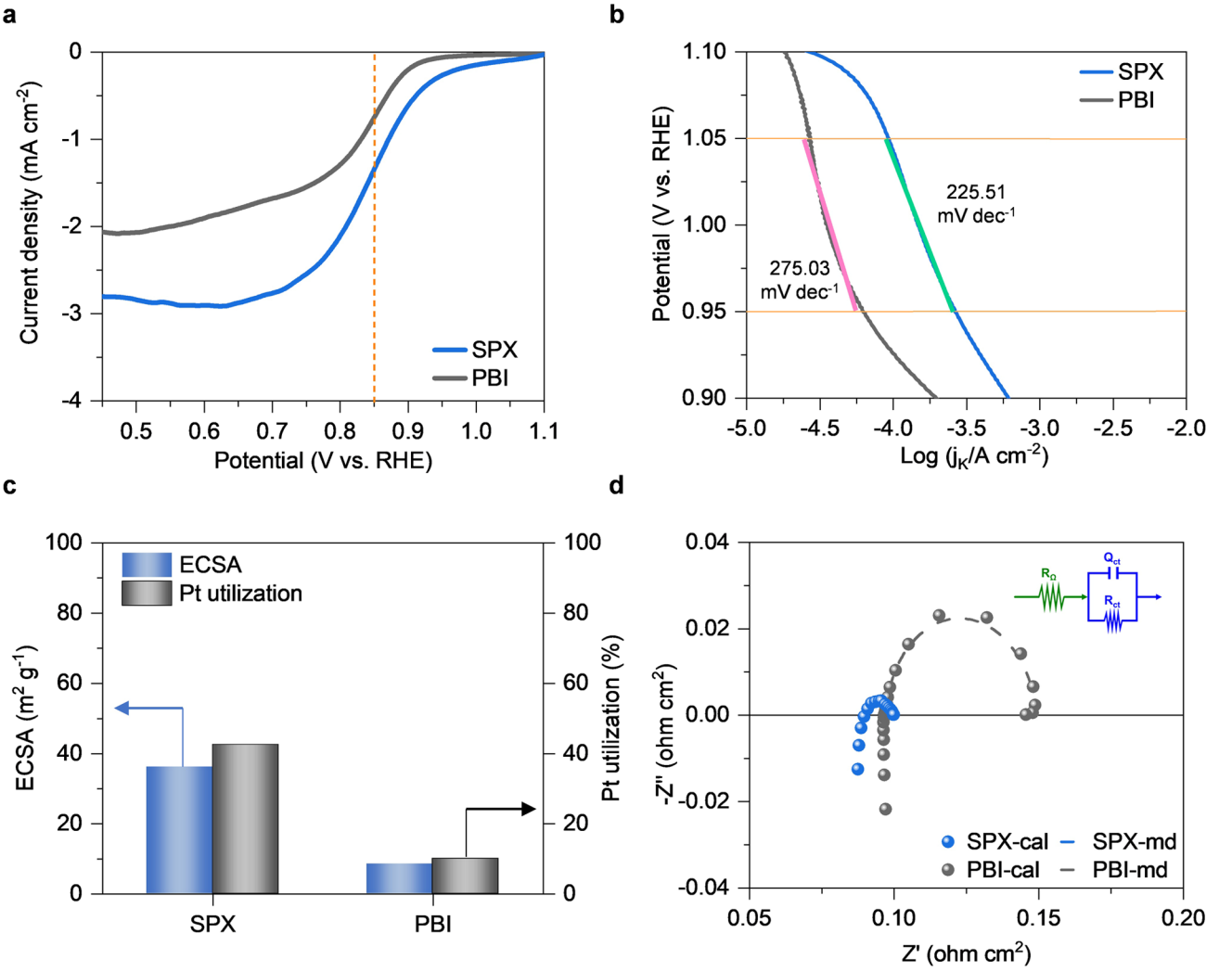

Figure 3. Electrochemical properties measured for SPX-based and PBI-based MEAs. (a) Linear sweep voltammograms (LSVs) and (b) Tafel curves of SPX-based and PBI-based MEAs obtained from TF-RDE at 1600 rpm. The Tafel slopes are indicated. (c) Pt utilization and electrochemical surface area (ECSA) of SPX-based and PBI-based MEAs calculated from the cyclic voltammograms. (d) Nyquist plots recorded at 160 °C and 0.6 V for MEAs prepared with SPX or PBI as the ionomeric binder, Pt/C (0.50 mg cm^{-2}) as catalysts, and PA-doped PBI as the membrane. The inset shows the equivalent electrical circuit model for EIS analysis. Measured data points are indicated by "-md", while calculation results are indicated by "-cal".

Pt surface (0−5 nm) (Figure 2a) shows that SPX has a relatively low density near the Pt catalyst surface, and the wide distribution indicates that SPX exhibits a weaker adsorption on the Pt surface and a more loosely packed chain conformation.

An appropriate electrode binder should facilitate rapid mass transport and help establish efficient triple-phase boundaries.[19] Dynamic vapor sorption (DVS) isotherms reveal a water sorption rate of 5.28×10^{-6} mg s^{-1} for SPX, while that of PBI is approximately 3.07×10^{-6} mg s^{-1} (Figure 2b). We then evaluate the transport of O_2 at the three-phase interface, considering that the permeability of H_2 through a typical PIM membrane is about 20 times that of O_2.[20] Molecular dynamics (MD) simulations were conducted to characterize the transport of O_2 across the SPX matrix and its distribution at the ionomer/catalyst interface. The three-dimensional O_2 density distribution map shows that most of the O_2 molecules can penetrate through the SPX film and distribute at the catalyst surface. By contrast, when PBI is used as the ionomeric binder, the transport of O_2 is blocked by the polymer film and cannot reach the catalyst surface (Figure 2c). Two-dimensional oxygen equilibrium snapshots confirm this observation (Figure S8). Interestingly, the O_2 molecules diffuse across the SPX ionomer/Pt catalyst interface at a relatively constant rate, whereas a plateau is observed in the PBI system (Figure S9a). This may be attributed to the accumulation of O_2 near the PBI film, which may lead to O_2 starvation at the Pt catalyst surface. We confirmed this assumption by comparing the oxygen density distributions near Pt. With SPX as the binder, 41% of O_2 can reach within 2 nm of the Pt catalyst, whereas the value is only 23% for the PBI system (Figure S9b). The O_2 permeation rate measured by a homemade gas permeation device also supports this conclusion (Figure S10). With the same thickness of 25 μm, for the SPX film, an O_2 permeation rate of 73.9 Barrer is obtained under an external pressure of 2 bar, while for the PBI film, an external pressure of 6 bar leads to an O_2 permeation rate of only 0.789 Barrer (Figure 2d).

MEA Electrochemical Properties

We employed the rotating disk electrode (RDE) experiments to reveal the effects of SPX and PBI binders on the electrode oxygen reduction reaction (ORR).[21] We recorded the linear

https://doi.org/10.1021/jacsau.4c00565
JACS Au 2024, 4, 3277−3283

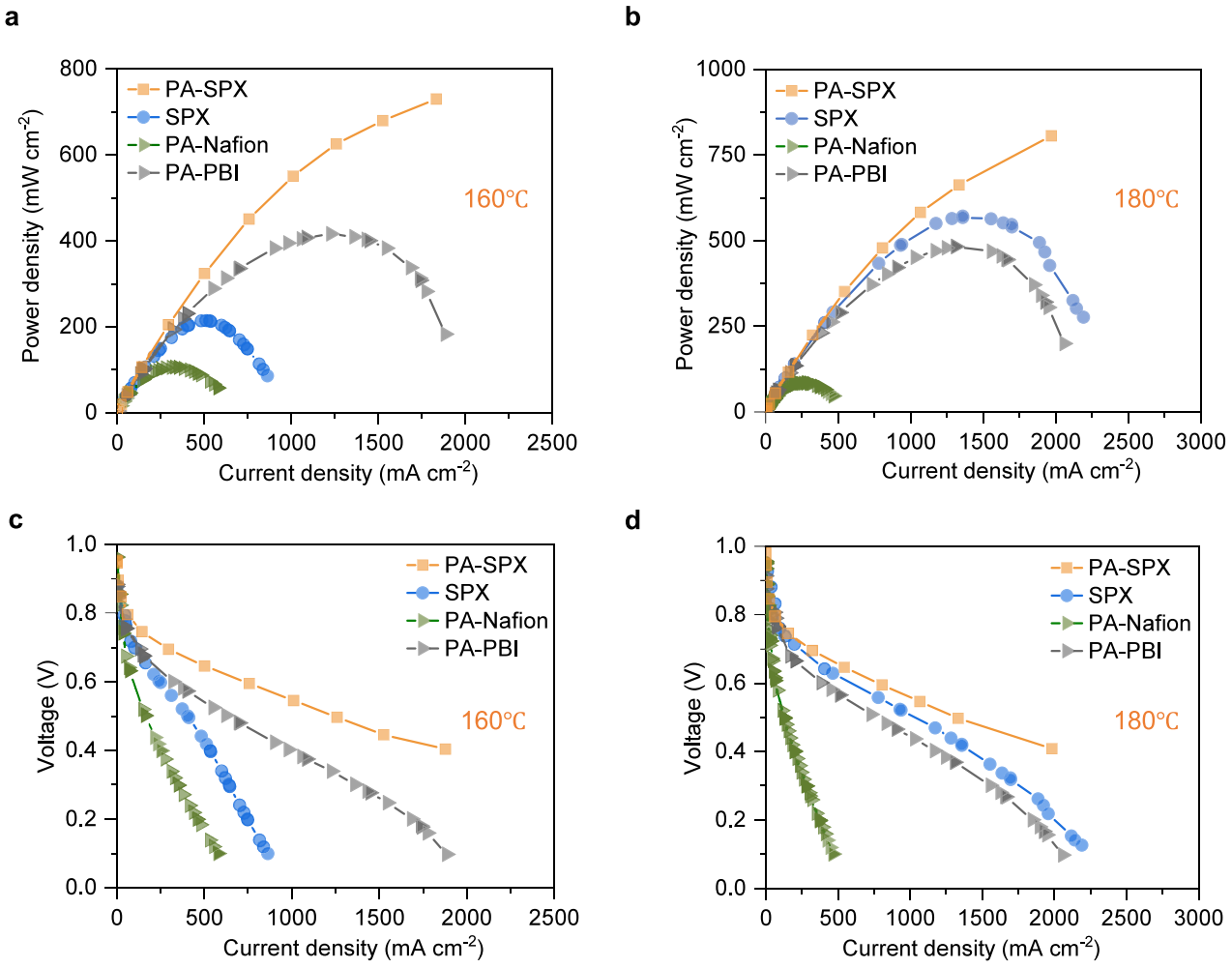

Figure 4. H_2/O_2 fuel cell performance. Power density of the H_2/O_2 fuel cell assembled with different ionomeric binders at (a) 160 and (b) 180 °C. Polarization curves of different ionomeric binders at (c) 160 °C and (d) 180 °C. The ionomeric binders include PA-SPX, SPX, PA-Nafion, and PA−PBI. H_2/O_2 flow rate: 0.5/0.5 L min^{-1}, without backpressure and under anhydrous conditions. Pt/C (0.50 mg cm^{-2}) as the catalyst and PA-doped PBI as the membrane.

sweep voltammograms (LSVs) of both SPX-based and PBI-based catalyst inks at different rotation speeds (Figure S11). We observed that under the same conditions, the half-wave potential ($E_{1/2}$) for both binder systems is 0.85 V, while a significantly different limiting current density (j_L) was observed.[22] The j_L is 2.77 mA cm^{-2} for the SPX-based catalyst ink, while it is only 2.07 mA cm^{-2} for the PBI-based catalyst ink (Figure 3a). We calculated the Tafel slopes of the two catalyst ink systems at a current density region where mass transport reaches the limit (Figure 3b). The rigid and twisted structure of the SPX ionomeric binder facilitates more efficient O_2 transport, resulting in a Tafel slope of 225.51 mV dec^{-1}, which is lower than that for the PBI system (275.03 mV dec^{-1}).

The electrochemically active surface area (ECSA) was derived from the cyclic voltammograms (CVs) of the SPX-based MEA and PBI-based MEA, assembled with the PA−PBI membrane, Pt/C catalyst, and SPX or PBI as the ionomeric binder (Figure S12, Figure 3c). The ECSA of the catalyst in the SPX-based MEA is 36.13 m^2 g^{-1}, with Pt utilization as high as 42.5%. By contrast, with PBI as the binder, the ECSA of the same catalyst is reduced to 8.49 m^2 g^{-1} and Pt utilization is less than 10%.

The reduction in interfacial charge transfer resistance (R_{ct}) is a key factor in improving the performance of fuel cells.[23,24] We measured the electrochemical impedance spectroscopy (EIS) of MEA to investigate the impact of the binders on MEA performance (Figure 3d). Since both MEAs use the same PA−PBI membrane, the total ohmic resistances (R_Ω) of the MEAs are similar. However, because of the high ECSA and Pt utilization enabled by SPX, the R_{ct} of the SPX-based MEA is 0.11 Ω cm^2, significantly lower than that of the PBI-based MEA (0.60 Ω cm^2, Table S1).

High-Temperature H_2/O_2 Fuel Cells

We tested the performance of MEAs assembled with SPX in high-temperature H_2/O_2 fuel cells. We evaluated the H_2/O_2 fuel cell performance at 160 °C, and the SPX-based MEA renders the corresponding cell a peak power density of 730 mW cm^{-2} at a current density of 1.83 A cm^{-2}, exceeding the 416 mW cm^{-2} peak power density achieved with PBI-based MEAs (Figure 4a). When the operating temperature was increased to 180 °C, the peak power density was increased to 805 mW cm^{-2} for the SPX-based MEA at a current density of 1.96 A cm^{-2} (Figure 4b). The improvement in the cell output power can be attributed to improved mass transport, as shown in Figure 4c. Since all MEAs used the same PA−PBI

https://doi.org/10.1021/jacsau.4c00565
JACS Au 2024, 4, 3277−3283

membrane and the same catalyst, their open-circuit voltages were similar (approximately 0.98 V). Similar voltage drops at a current below 0.3 V cm^{-2} were observed. However, at a current density range of 0.3 to 1.5 A cm^{-2}, limitations due to mass transport arise. At 1.5 A cm^{-2}, the voltage of the SPX-based MEA is 0.45 V, while it is 0.27 V for the PBI-based MEA, probably due to the differences in conductivity within the catalyst layer. A similar trend is maintained at 180 °C (Figure 4d). The above results support our hypothesis that using SPX as an ionomeric binder can facilitate mass transport and improve fuel cell performance.

Our control experiments show that PA with the SPX-based MEA is critical for a high cell performance. When no PA is added to the electrode and only a small amount of PA migrates from the membrane to the electrode, the cell performance is poor. We also found that when Nafion is used as a binder, its poor acid absorption properties cause PA to leach out easily, combined with the strong adsorption of sulfonic groups on Pt surfaces, resulting in the worst cell performance.[25,26]

We tested the H_2/O_2 fuel cell performance at temperatures ranging from 160 to 220 °C (Figure S13a,b). As the operating temperature is elevated from 160 to 180 °C, the peak power density slightly increases from 730 to 805 mW cm^{-2}. Surprisingly, as the temperature continues to rise to 200 °C, the output peak power declines to 552 mW cm^{-2}, which further drops to 490 mW cm^{-2} at 220 °C. This decline may be due to the formation of pyrophosphoric anhydride at temperatures above 180 °C, severely compromising proton conduction.[27,28]

We also attempted to reduce the catalyst loading in the SPX-based MEA. When the Pt loading was reduced to 0.3 mg cm^{-2}, the peak power density was suboptimal (Figure S13c,d). This could be attributed to the poisoning effect of phosphate anions within the electrode on the Pt catalyst.[29,30] At this stage, reducing the catalyst loading results in insufficient active sites for electrode reactions, and further efforts are thus demanded.

CONCLUSIONS

In summary, we investigated the changes brought about by using sulfonated microporous polymer SPX as a binder for HT-PEMFCs based on the PA-doped PBI membrane. This polymer features a rigid and contorted backbone, preventing effective polymer chain packing and resulting in abundant free volume elements. The adoption of SPX as a binder enhances mass transport within the MEA, benefiting from the abundant free volume and microporous channels, which allow fast transport of reactant gases and product water. The microporous channels also enhance PA retention and facilitate proton conduction. Molecular simulations demonstrate that the rigid, twisted molecular conformation of the SPX ionomer significantly reduces its adsorption on the Pt catalyst surface. The above characteristics of SPX improve electrode reaction kinetics, reduce mass transfer resistance, and increase Pt utilization (~42.5%). The MEA assembled with SPX as the binder achieved a peak power density of 805 mW cm^{-2} at 180 °C, far exceeding that with PBI. In conclusion, our theoretical and experimental studies indicate that sulfonated microporous polymer SPX is an ideal choice for a catalyst layer binder. This concept may be broadly applicable to other types of electrode reactions involving a three-phase boundary. Future efforts should be devoted to further improving the thermal stability of SPX, ideally to withstand temperatures above 250 °C and prevent anhydride formation within the MEA at temperatures above 200 °C.

ASSOCIATED CONTENT

Supporting Information

The Supporting Information is available free of charge at https://pubs.acs.org/doi/10.1021/jacsau.4c00565.

Additional experimental details, materials, methods, and extraction results including ^1H NMR spectra, N_2 sorption adsorption−desorption isotherms, pore size distributions, adsorption energies, cumulative pore volume distributions, O_2 equilibrium snapshots, LSV for the catalyst inks, CV curves for the catalyst inks, and in situ electrochemical analyses of the MEAs (PDF)

AUTHOR INFORMATION

Corresponding Authors

Zhengjin Yang − *Key Laboratory of Precision and Intelligent Chemistry and Department of Applied Chemistry, School of Chemistry and Materials Science, University of Science and Technology of China, Hefei 230026, China;* orcid.org/0000-0002-0722-7908; Email: yangzj09@ustc.edu.cn

Tongwen Xu − *Key Laboratory of Precision and Intelligent Chemistry and Department of Applied Chemistry, School of Chemistry and Materials Science, University of Science and Technology of China, Hefei 230026, China;* orcid.org/0000-0002-9221-5126; Email: twxu@ustc.edu.cn

Authors

Shuo Yang − *Key Laboratory of Precision and Intelligent Chemistry, University of Science and Technology of China, Hefei 230026, China; Institute of Advanced Technology, University of Science and Technology of China, Hefei 230026, China*

Hui Li − *Key Laboratory of Precision and Intelligent Chemistry and Department of Applied Chemistry, School of Chemistry and Materials Science, University of Science and Technology of China, Hefei 230026, China*

Wenhao Zou − *Key Laboratory of Precision and Intelligent Chemistry and Department of Applied Chemistry, School of Chemistry and Materials Science, University of Science and Technology of China, Hefei 230026, China*

Rene Ling − *Key Laboratory of Precision and Intelligent Chemistry and Department of Applied Chemistry, School of Chemistry and Materials Science, University of Science and Technology of China, Hefei 230026, China*

Xinchi Ma − *Key Laboratory of Precision and Intelligent Chemistry, University of Science and Technology of China, Hefei 230026, China; Department of Polymer Science and Engineering, School of Chemistry and Material Science, University of Science and Technology of China, Hefei 230026, China*

Siyu Chen − *Key Laboratory of Precision and Intelligent Chemistry, University of Science and Technology of China, Hefei 230026, China; Department of Polymer Science and Engineering, School of Chemistry and Material Science, University of Science and Technology of China, Hefei 230026, China*

Complete contact information is available at: https://pubs.acs.org/10.1021/jacsau.4c00565

Author Contributions

⊥S.Y. and H.L. contributed equally. Z.Y. and T.X. supervised this work. Z.Y., S.Y., and H.L. conceived this project and wrote the paper. Z.Y., S.Y., and H.L. performed all the experiments and data analysis. W.Z. carried out the DFT calculation. R.L., X.M., and S.C. assisted in the result discussion.

Notes

The authors declare no competing financial interest.

■ ACKNOWLEDGMENTS

This work was funded by the National Natural Science Foundation of China (Grant/Award Numbers: U20A20127 and 21922510). This work was partially carried out at the Instruments Center for Physical Science, University of Science and Technology of China.

■ REFERENCES

(1) Schonvogel, D.; Büsselmann, J.; Schmies, H.; Langnickel, H.; Wagner, P.; Dyck, A. High temperature polymer electrolyte membrane fuel cell degradation provoked by ammonia as ambient air contaminant. *J. Power Sources* **2021**, *502*, No. 229993.

(2) Bose, S.; Kuila, T.; Nguyen, T. X. H.; Kim, N. H.; Lau, K.; Lee, J. H. Polymer membranes for high temperature proton exchange membrane fuel cell: Recent advances and challenges. *Prog. Polym. Sci.* **2011**, *36*, 813−843.

(3) Aili, D.; Henkensmeier, D.; Martin, S.; Singh, B.; Hu, Y.; Jensen, J. O.; Cleemann, L. N.; Li, Q. Polybenzimidazole-Based High-Temperature Polymer Electrolyte Membrane Fuel Cells: New Insights and Recent Progress. *Electrochem. Energy Rev.* **2020**, *3*, 793−845.

(4) Wu, Z.; Shan, S.; Zang, S.; Zhong, C. Dynamic Core−Shell and Alloy Structures of Multimetallic Nanomaterials and Their Catalytic Synergies. *Acc. Chem. Res.* **2020**, *53*, 2913−2924.

(5) Park, J. O.; Kwon, K.; Cho, M. D.; Hong, S. G.; Kim, T. Y.; Yoo, D. Y. Role of Binders in High Temperature PEMFC Electrode. *J. Electrochem. Soc.* **2011**, *158*, B675−B681.

(6) Jung, J.; Ku, J.; Park, Y. S.; Ahn, C.; Lee, J.; Hwang, S. S.; Lee, A. S. Advances in Ion Conducting Membranes and Binders for High Temperature Polymer Electrolyte Membrane Fuel Cells. *Polym. Rev.* **2022**, *62*, 789−825.

(7) Favero, S.; Stephens, I. E. L.; Titirci, M. Anion Exchange Ionomers: Design Considerations and Recent Advances - An Electrochemical Perspective. *Adv. Mater.* **2023**, *36*, No. e2308238.

(8) Tang, M.; Zhang, S.; Chen, S. Pt utilization in proton exchange membrane fuel cells: structure impacting factors and mechanistic insights. *Chem. Soc. Rev.* **2022**, *51*, 1529−1546.

(9) Mamlouk, M.; Scott, K. The effect of electrode parameters on performance of a phosphoric acid-doped PBI membrane fuel cell. *Int. J. Hydrog. Energy* **2010**, *35*, 784−793.

(10) Smith, K.; Foglia, F.; Clancy, A. J.; Brett, D. J. L.; Miller, T. S. Nafion Matrix and Ionic Domain Tuning for High-Performance Composite Proton Exchange Membranes. *Adv. Funct. Mater.* **2023**, *33*, No. 2304061.

(11) Li, D.; Chung, H. T.; Maurya, S.; Matanovic, I.; Kim, Y. S. Impact of ionomer adsorption on alkaline hydrogen oxidation activity and fuel cell performance. *Curr. Opin. Electrochem.* **2018**, *12*, 189−195.

(12) Mack, F.; Morawietz, T.; Hiesgen, R.; Kramer, D.; Zeis, R. PTFE Distribution in High-Temperature PEM Electrodes and Its Effect on the Cell Performance. *ECS Trans.* **2013**, *58*, 881−888.

(13) Tang, H.; Geng, K.; Aili, D.; Ju, Q.; Pan, J.; Chao, G.; Yin, X.; Guo, X.; Li, Q.; Li, N. Low Pt loading for high-performance fuel cell electrodes enabled by hydrogen-bonding microporous polymer binders. *Nat. Commun.* **2022**, *13*, 7577.

(14) Budd, P. M.; Elabas, E. S.; Ghanem, B. S.; Makhseed, S.; McKeown, N. B.; Msayib, K. J.; Tattershall, C. E.; Wang, D. Solution-Processed, Organophilic Membrane Derived from a Polymer of Intrinsic Microporosity. *Adv. Mater.* **2004**, *16*, 456−459.

(15) Zhang, Q.; Dong, S.; Shao, P.; Zhu, Y.; Mu, Z.; Sheng, D.; Zhang, T.; Jiang, X.; Shao, R.; Ren, Z.; Xie, J.; Feng, X.; Wang, B. Covalent organic framework-based porous ionomers for high-performance fuel cells. *Science* **2022**, *378*, 181−186.

(16) Zuo, P.; Li, Y.; Wang, A.; Tan, R.; Liu, Y.; Liang, X.; Sheng, F.; Tang, G.; Ge, L.; Wu, L.; Song, Q.; McKeown, N. B.; Yang, Z.; Xu, T. Sulfonated Microporous Polymer Membranes with Fast and Selective Ion Transport for Electrochemical Energy Conversion and Storage. *Angew. Chem., Int. Ed.* **2020**, *59*, 9564−9573.

(17) Xue, B.; Zheng, Z.; Qian, H.; Wang, Z.; Yan, J. Robust Proton-Exchange Membranes Based on Perfluorosulfonic Acid-Functionalized Poly(phenyl-alkane) and Polyxanthene: Effects of Skeletal Structures on Membrane Properties. *Macromolecules* **2024**, *57*, 3376−3386.

(18) Maurya, S.; Noh, S.; Matanovic, I.; Park, E. J.; Villarrubia, C. N.; Martinez, U.; Han, J.; Bae, C.; Kim, Y. S. Rational design of polyaromatic ionomers for alkaline membrane fuel cells with > 1 W cm^{-2} power density. *Energy Environ. Sci.* **2018**, *11*, 3283−3291.

(19) Kim, D.; Jung, H.; Chun, H.; Pak, C. Enhanced membrane electrode assembly performance by adding PTFE/Carbon black for high temperature polymer electrolyte membrane fuel cell. *Int. J. Hydrog. Energy* **2021**, *46*, 29424−29431.

(20) Carta, M.; Malpass-Evans, R.; Croad, M.; Rogan, Y.; Jansen, J. C.; Bernardo, P.; Bazzarelli, F.; McKeown, N. B. An Efficient Polymer Molecular Sieve for Membrane Gas Separations. *Science* **2013**, *339*, 303−307.

(21) Xia, Y.; Guo, P.; Li, J.; Zhao, L.; Sui, X.; Wang, Y.; Wang, Z. How to appropriately assess the oxygen reduction reaction activity of platinum group metal catalysts with rotating disk electrode. *IScience* **2021**, *24*, No. 103024.

(22) Garsany, Y.; Baturina, O. A.; Swider-Lyons, K. E.; Kocha, S. S. Experimental Methods for Quantifying the Activity of Platinum Electrocatalysts for the Oxygen Reduction Reaction. *Anal. Chem.* **2010**, *82*, 6321−6328.

(23) Leu, H.; Chiu, K.; Lin, C. Smart coating process of proton-exchange membrane for polymer electrolyte fuel cell. *Appl. Energy* **2013**, *112*, 1126−1130.

(24) Chen, Y. R.; Chiu, K. F.; Chen, C. L.; Lin, H. C.; Chang, W. Y.; Tsai, C. B.; Ho, W. H. Thin catalyst layer deposited on proton-exchange membrane by self-breathing method. *Surf. Coat. Technol.* **2013**, *231*, 112−116.

(25) Chen, F.; Chen, S.; Wang, A.; Wang, M.; Guo, L.; Wei, Z. Blocking the sulfonate group in Nafion to unlock platinum's activity in membrane electrode assemblies. *Nat. Catal.* **2023**, *6*, 392−401.

(26) Modestino, M. A.; Paul, D. K.; Dishari, S.; Petrina, S. A.; Allen, F. I.; Hickner, M. A.; Karan, K.; Segalman, R. A.; Weber, A. Z. Self-Assembly and Transport Limitations in Confined Nafion Films. *Macromolecules* **2013**, *46*, 867−873.

(27) Seselj, N.; Aili, D.; Celenk, S.; Cleemann, L. N.; Hjuler, H. A.; Jensen, J. O.; Azizi, K.; Li, Q. Performance degradation and mitigation of high temperature polybenzimidazole-based polymer electrolyte membrane fuel cells. *Chem. Soc. Rev.* **2023**, *52*, 4046−4070.

(28) Li, H.; Zuo, P.; Wu, W.; Tang, G.; Fang, J.; Xu, T.; Yang, Z. Electrode binder design for high-power, low-Pt loading and durable high temperature fuel cells. *Energy Environ. Sci.* **2024**, *17*, 3651−3659.

(29) Kaserer, S.; Caldwell, K. M.; Ramaker, D. E.; Roth, C. Analyzing the Influence of H_3PO_4 as Catalyst Poison in High Temperature PEM Fuel Cells Using in - operando X-ray Absorption Spectroscopy. *J. Phys. Chem. C* **2013**, *117*, 6210−6217.

(30) Prokop, M.; Bystron, T.; Bouzek, K. Electrochemistry of Phosphorous and Hypophosphorous Acid on a Pt electrode. *Electrochim. Acta* **2015**, *160*, 214−218.

https://doi.org/10.1021/jacsau.4c00565
JACS Au 2024, 4, 3277−3283